Banner appropriate to article type will appear here in typeset article

Sound wave propagation in rarefied molecular gases

Shaokang Li[1], Wei Su[2,3] and Yonghao Zhang[4]†

[1]School of Engineering, The University of Edinburgh, Edinburgh EH9 3FB, United Kingdom

[2]Division of Emerging Interdisciplinary Areas, The Hong Kong University of Science and Technology, Hong Kong, China

[3]Department of Mathematics, The Hong Kong University of Science and Technology, Hong Kong, China

[4]State Key Laboratory of High-Temperature Gas Dynamics, Institute of Mechanics, Chinese Academy of Sciences, Beijing 100190, China

Sound wave propagation in rarefied flows of molecular (diatomic and polyatomic) gases confined in micro-channels is numerically investigated. We first validate the employed kinetic model against the experimental results, then systematically study the gas damping and surface force on the transducer, as well as the resonance/anti-resonance in confined space. To quantify the impact of the finite relaxation rates of the translational and internal energies on wave propagation, we elaborate on the roles of bulk viscosity and thermal conductivity in depth over a wide range of rarefactions and oscillation frequencies. It is found that the bulk viscosity only exerts influence on pressure amplitude and its resonance frequency in the slip regime in high oscillation. And the internal degree of freedom is frozen when the bulk viscosity of a molecular gas is large, resulting in the pressure amplitude of sound waves in the molecular gas being the same as those in a monatomic gas. Meanwhile, the thermal conductivity has a limited influence on the pressure amplitude in all the simulated flows. In the case of the thermoacoustic wave, we prove that the Onsager-Casimir reciprocal relation also holds for molecular gases, i.e., the pressure deviation induced by the temperature variation is equal to the heat flux induced by plate oscillation. Our findings provide an enhanced understanding of sound wave propagation in molecular gases which may facilitate the design of nano-/micro-scales devices.

Key words: rarefied gas dynamics, kinetic theory, sound wave, resonance, molecular gases

1. Introduction

Sound wave propagation at nano-/micro-scales plays a key role in a variety of applications, e.g., vibrating micromechanical resonators in on-chip communication devices (Clark *et al.* 2005), acoustic transducers in micro-electro-mechanical-system (MEMS) sensors such as gyroscopes and accelerometers, and porous acoustic absorber for sound reduction (Yang

† Email address for correspondence: yonghao.zhang@imech.ac.cn

& Sheng 2017). Since the geometric size shrinks to nano/micrometers and the surface-to-volume ratio dramatically increases, gas rarefaction and surface effects such as gas damping are significantly enhanced, which largely determine the devices' performance (Chigullapalli *et al.* 2012). For instance, the Brownian noise level in a MEMS accelerometer is dominated by the gas damping in its capacitive transducers (Boom *et al.* 2021); the efficiency of sound absorbing in an acoustic absorber is low when gas damping is weak. Therefore, understanding rarefied gas damping and gas-surface interaction in vibrating MEMS and porous structures is of great importance for the design and operation of these nano-/micro-devices. Moreover, as gases are encompassed in a confined space, resonance and anti-resonance can induce local extreme pressure amplitudes, which is another important issue to be considered carefully (Struchtrup 2012).

In addition to miniaturization in size, high-frequency of a sound wave will also generate rarefaction effects. Therefore, two Knudsen numbers are often introduced to quantify the degree of rarefaction, i.e. the length-based Knudsen number (Kn_l), defined as the ratio of the mean free path of gas molecules to the characteristic flow length, and the time-based Knudsen number (Kn_t), the ratio between the molecular mean free time and the process time scale. The traditional Navier-Stokes equations are adequate to describe gas flows only when both Knudsen numbers are small, say, $Kn_{l/t} < 0.001$; otherwise, like the flow conditions often found in nano-/micro devices (Park *et al.* 2004; Frangi *et al.* 2007; Wang *et al.* 2018), gas kinetic theory is necessarily adopted to predict flow properties (Sharipov & Kalempa 2008; Kalempa & Sharipov 2009).

The kinetic theory has been exploited to investigate sound wave propagation in rarefied gases confined in nano-/micro-channels. Through the solution of the Boltzmann equation or its simplified kinetic model equations, the gas damping properties including the spatial variations of pressure amplitude, temperature and heat flux have been reported under different oscillation frequencies and amplitudes (Garcia & Siewert 2005; Wang & Xu 2012). The resonance induced by the superposition of waves is also investigated (Desvillettes & Lorenzani 2012; Wu *et al.* 2014). At the high-frequency limit where molecular collisions during the characteristic flow time scale can be ignored, analytical solutions of the resonance and anti-resonance frequencies have been obtained for one-dimensional and two-dimensional channel flows. Noticed that most of the aforementioned studies focused on monatomic gases (Bisi & Lorenzani 2016), nevertheless, the most common working gas is air, mainly composed of nitrogen and oxygen. Modelling of sound wave propagation in molecular (diatomic and polyatomic) gases is more difficult since the kinetic equation describing the dynamics of rarefied flows of molecular gases is much more complex than the Boltzmann equation. Compared to monatomic gases, the molecules of a molecular gas possess internal degrees of freedom due to the excitation of rotational, vibrational, and electronic modes. The finite rates of the relaxation processes regarding translational and internal modes lead to more complex non-equilibrium phenomena. For instance, a new transport coefficient, i.e., the bulk viscosity emerges (Mandelshtam & Leontovich 1937; Tisza 1942); meanwhile, the thermal conductivity contains not only the translational contribution but also internal components (Eucken 1913). Previous studies showed that the bulk viscosity is determined by the relaxation rate between the translational and internal energies, and the translational and internal thermal conductivities are respectively determined by the relaxation rates of the translational and internal heat fluxes. These additional transport mechanisms, however, can significantly affect the flow properties of rarefied molecular gases such as the shock-wave structure (Kosuge & Aoki 2018), the line shape of the Rayleigh-Brillouin scattering (Wu *et al.* 2020) and the flow velocity of the thermal transpiration in micro-channels (Li *et al.* 2021; Su *et al.* 2021). Some works have been done to assess the properties of sound wave propagation in molecular gases of single or multiple components, where the influence of

the energy exchange among different modes on the attenuation and phase velocity was addressed (Dain & Lueptow 2001*a,b*; Ejakov *et al.* 2003; Rahimi & Struchtrup 2014; Arima *et al.* 2017; Kremer *et al.* 2018; Kustova *et al.* 2023). The investigations were mainly based on continuum equations, including the Euler, Navier-Stokes, Grad's moment, and rational extended thermodynamic equations. The non-equilibrium dynamics of the relaxation of internal energies were modelled by additional relaxation equations according to the multi-temperature method or state-specific description. The acoustic behaviour of the attenuation coefficient with respect to the energy relaxation rate, gas species, and sound frequency was obtained and compared with experimental measurements. The acoustic properties of the wave propagation were considered in homogeneous flows, thus, gas damping due to the gas-surface interaction and resonance in confined space are not included. Noticed that, if the Euler/Navier-Stokes or moment equations are applied, it is implied that the flow characteristic time scale is much larger than the mean free time of gas molecules (or translation relaxation time); that is Kn_t should be small enough (Rahimi & Struchtrup 2014).

To the authors' best knowledge, a systemic study has yet to be conducted, focusing on the effects of bulk viscosity (i.e., finite relaxation rate of translational and internal energies) and thermal conductivity (i.e., finite relaxation rate of translational and internal heat fluxes) on the sound wave propagation in confined channels, particularly under a wide range of Knudsen numbers and sound frequencies. In this work, we will fill this knowledge gap and reveal some unique propagation properties in rarefied molecular gases. In addition to sound wave propagation, propagation of thermoacoustic wave induced by periodic variation of temperature is also important to many engineering applications, e.g., Pirani gauges, used to measure pressure in vacuum systems (Kalempa & Sharipov 2014). The Onsager-Casimir reciprocal relation (OCRR), an important principle that links thermodynamics fluxes driven by different forces (Onsager 1931*a,b*; Casimir 1945), becomes a powerful tool to validate simulation and measurement results and reduce the computational cost and the number of required experimental measurements. Previously, a general approach has been proposed to demonstrate OCRR for the rarefied flow of monatomic gases (Sharipov 2006; Kalempa & Sharipov 2012). In this work, we will examine whether the OCRR holds for molecular gases.

The remainder of this paper is organized as follows: the kinetic model and boundary conditions are described in Section 2; the formulation of wave propagation will be presented in Section 3; in Section 4, we will first validate the model against the experimental data, and then investigate influence of the unique transport coefficients of molecular gases on gas damping, surface force, and resonance. Before concluding the work, we will numerically prove that OCRR also holds for sound and thermal-acoustic wave propagation in molecular gases.

2. Kinetic model

The Boltzmann equation was extended for molecular gases by Wang-Chang & Uhlenbeck (1951) considering quantum mechanics where each internal energy level is assigned with an individual velocity distribution function; this yields a complicated operator for particle collisions that is prohibitively expensive for numerical simulations. Several simplified models using the relaxation-time approach have been developed (Morse 1964; Holway & Lowell 1966; Rykov 1975; Gorji & Jenny 2013; Wu *et al.* 2015; Wang *et al.* 2017). Generally, rarefied gas damping and resonance problems can be investigated by seeking solutions of kinetic equations via the direct simulation Monte Carlo (DSMC) (Hadjiconstantinou 2002; Emerson *et al.* 2007) method or the discrete velocity method (DVM) (Kalempa & Sharipov 2009; Wu *et al.* 2014). The DSMC method uses a collection of particles to mimic the behaviour of gas molecules: particles move through the spatial space in a realistic manner,

while intermolecular collisions and gas-interactions are calculated stochastically according to some collision models and pair-selection schemes (Bird 1994; Ivanov & Rogasinskii 1991; Roohi *et al.* 2018). It was rigorously proved that the DSMC and the Boltzmann equation are equivalent for monatomic gases (Wagner 1992). For rarefied molecular gases, the Borgnakke & Larsen (1975) phenomenological collision model was developed to reproduce the energy exchange rate, where one continuous variable was introduced to represent the internal energies of a molecular gas. Although the DSMC is widely used simulation technique for rarefied gas flows, it is very time-consuming for oscillating problems (Park *et al.* 2004). The time step has to be significantly small (compared to both the molecular mean free time and the time period of oscillations) and the total simulation time should be sufficiently long to ensure the time-periodic state is achieved. Besides, in an unsteady DSMC algorithm, ensemble averaging over thousands of different simulations for each time step is necessary to yield noise-reduced solutions.

The DVM, on the other hand, falls into deterministic approaches. It relies on direct direcretisation of the governing equation over computational grids, thus, can produce noise-free solutions. Furthermore, by assuming small variations in flow properties, the time-periodic flow can be converted into a quasi steady-state problem and the computational cost will be largely reduced (see Section 3). Therefore, in this work, we use the DVM and a deterministic-based model (Li *et al.* 2021; Su *et al.* 2022) to investigate wave propagation in rarefied molecular gases, which is modified from the Rykov model (Rykov 1975). The model is able to recover the general temperature and thermal relaxation rates that are predicted by the Wang-Chang-Uhlenbeck equation and can freely adjust the relevant relaxation rates. Therefore, it can simultaneously obtain experimentally measured values of the bulk viscosity and thermal conductivity for a given molecular gas (Wu *et al.* 2020; Li *et al.* 2021; Su *et al.* 2022), and their affects on the wave propagation can be separately investigated. To avoid too many parameters in the analysis, we assume that vibrations of a molecule are not activated. This assumption has limitations for some polyatomic gases such as carbon dioxide and methane, where vibrational relaxation plays a crucial role in wave attenuation (Ejakov *et al.* 2003; Kustova *et al.* 2023). In such cases, a model taking into account both rational and vibrational relaxations (Li *et al.* 2023) is necessary, where additional relaxation rates are required. The rotational mode is considered through the classical mechanics approach, with a continuous variable representing the rotational energy. A brief description of the present kinetic model is given below.

In the gas kinetic theory, the state of a molecular gas with the excited rotational mode is described by a one-particle velocity-energy distribution function $f(t, \boldsymbol{x}, \boldsymbol{v}, I)$, which is a function of time t, spatial coordinate $\boldsymbol{x} = (x, y, z)$, molecular translational velocity $\boldsymbol{v} = (v_x, v_y, v_z)$, and rotational energy I. In the absence of external force, the evolution of f is governed by (Rykov 1975; Su *et al.* 2022)

$$\frac{\partial f}{\partial t} + \boldsymbol{v} \cdot \frac{\partial f}{\partial \boldsymbol{x}} = \underbrace{\frac{p_t \delta_0}{\mu} (g_t - f)}_{\text{elastic}} + \underbrace{\frac{p_t \delta_0}{\mu Z} (g_r - g_t)}_{\text{inelastic}}. \tag{2.1}$$

It can be seen that the collision operator (the term on the right-hand side) that describes the change of f due to particle collisions is split into two parts: the elastic collisions that preserve translational energy and the inelastic ones that exchange translational and rotational energies. Both elastic and inelastic parts are expressed as a simple relaxation term, where the relaxation time related to elastic collisions is $\mu/(p_t \delta_0)$ with μ, p_t and δ_0 being gas shear viscosity, pressure related to translational motions, and a constant rarefaction parameter, respectively. Z is the rotational collision number such that a gas molecule would roughly

177 experience one inelastic collision in every Z collisions. g_t and g_r are the translational
178 and rotational reference distribution functions, respectively. The reference distributions are
179 series of orthogonal polynomials, expanding at the local equilibrium distribution function E
180 $= E_t(T) \cdot E_r(T)$, read as

$$g_t = E_t(T_t) \cdot E_r(T_r) \left[1 + \frac{4\boldsymbol{q}_t \cdot \boldsymbol{c}}{15T_t p_t} \left(\frac{|\boldsymbol{c}|^2}{T_t} - \frac{5}{2} \right) + \frac{4\boldsymbol{q}_r \cdot \boldsymbol{c}}{dT_t p_r} \left(\frac{I}{T_r} - \frac{d}{2} \right) \right], \tag{2.2}$$

$$g_r = E_t(T) \cdot E_r(T) \left[1 + \frac{4\boldsymbol{q}' \cdot \boldsymbol{c}}{15T p} \left(\frac{|\boldsymbol{c}|^2}{T} - \frac{5}{2} \right) + \frac{4\boldsymbol{q}'' \cdot \boldsymbol{c}}{dT p} \left(\frac{I}{T} - \frac{d}{2} \right) \right], \tag{2.3}$$

183 with E_t and E_r being the local Maxwellian distributions

$$E_t(T) = \frac{n}{(\pi T)^{3/2}} \exp\left(-\frac{|\boldsymbol{c}|^2}{T} \right), \tag{2.4}$$

$$E_r(T) = \frac{I^{d/2-1}}{\Gamma(d/2) T^{d/2}} \exp\left(-\frac{I}{T} \right). \tag{2.5}$$

187 In the above formula, d is the number of rotational degrees of freedom; $\Gamma(\cdot)$ is the gamma
188 function; T_t, T_r, $\boldsymbol{q}_t = \left(q_t^x, q_t^y, q_t^z \right)$, and $\boldsymbol{q}_r = \left(q_r^x, q_r^y, q_r^z \right)$ are the translational and rotational
189 temperatures, and the related heat fluxes, respectively; and $\boldsymbol{c} = \boldsymbol{v} - \boldsymbol{u}$ is the peculiar velocity
190 with $\boldsymbol{u} = (u_x, u_y, u_z)$ being gas bulk velocity. The overall temperature T is a weighted sum
191 of the translational and rotational temperatures: $T = (3T_t + dT_r) / (3 + d)$. The pressures
192 are defined as $p_t = nT_t$, and $p = nT$ in terms of the translational, and overall temperatures,
193 respectively; here n is gas number density. $\boldsymbol{q}'$ and $\boldsymbol{q}''$ are two auxiliary heat fluxes, introduced
194 as the linear combinations of the translational and rotational heat fluxes (Li *et al.* 2021)

$$\begin{bmatrix} \boldsymbol{q}' \\ \boldsymbol{q}'' \end{bmatrix} = \begin{bmatrix} (2 - 3A_{tt})Z + 1 & -3A_{tr}Z \\ -A_{rt}Z & 1 - A_{rr}Z \end{bmatrix} \begin{bmatrix} \boldsymbol{q}_t \\ \boldsymbol{q}_r \end{bmatrix}, \tag{2.6}$$

196 where A_{ij} ($i, j = t$ or r) are the thermal relaxation rates.
197 Here, density and temperatures are normalized by the reference density n_0 and temperature
198 T_0, respectively; shear viscosity, by its value at the reference temperature μ_0; velocities, by
199 the most probable speed $v_m = \sqrt{2k_B T_0/m}$ where k_B is the Boltzmann constant and m is the
200 molecular mass; spatial coordinates, by the characteristic flow length H; time, by H/v_m; the
201 internal energy, by $k_B T_0$; heat fluxes, by $n_0 k_B T_0 v_m$; pressures, by $n_0 k_B T_0$; and the distribution
202 functions, by $n_0 v_m^{-3} (k_B T_0)^{-1}$. The rarefaction parameter is therefore defined as

$$\delta_0 = \frac{p_0 H}{\mu_0 v_m}, \tag{2.7}$$

204 where $p_0 = n_0 k_B T_0$. It is inversely proportional to the unconfined length-based Knudsen
205 number:

$$\mathrm{Kn}_l = \frac{\sqrt{\pi}}{2} \frac{1}{\delta_0}. \tag{2.8}$$

207 It is straightforward to show that the kinetic model recovers the Jeans-Landau temperature
208 relaxation model, i.e.,

$$\frac{\partial T_r}{\partial t} = \frac{p_t \delta_0}{\mu Z} (T - T_r). \tag{2.9}$$

210 In addition, the heat flux relaxation of the present model are consistent with the one derived
211 from the Wang-Chang Uhlenbeck equation by Mason & Monchick (1962). The heat flux

212 relaxation directly determines the thermal conductivity, as well as the translational and
213 rotational contributions (Mason & Monchick 1962; McCormack 1968), i.e.,

$$
214 \quad \left[\begin{array}{c} \partial \boldsymbol{q}_t / \partial t \\ \partial \boldsymbol{q}_r / \partial t \end{array} \right] = -\frac{p_t \delta_0}{\mu} \left[\begin{array}{cc} A_{tt} & A_{tr} \\ A_{rt} & A_{rr} \end{array} \right] \left[\begin{array}{c} \boldsymbol{q}_t \\ \boldsymbol{q}_r \end{array} \right]. \tag{2.10}
$$

215 Applying the Chapman-Enskog multiscale expansion to the kinetic model equation and
216 retaining the terms up to the order of $O(1/\delta)$, the Navier-Stokes equations can be derived,
217 and the transport coefficients are immediately obtained. The dimensionless bulk viscosity
218 μ_b (normalised by μ_0) is read as

$$
219 \quad \mu_b = \frac{2dZ}{3(d+3)} \mu, \tag{2.11}
$$

220 while the dimensionless translational conductivity κ_t and rotational conductivity κ_r (nor-
221 malised by $2k_B\mu_0/m$) are determined as

$$
222 \quad \left[\begin{array}{c} \kappa_t \\ \kappa_r \end{array} \right] = \frac{\mu}{4} \left[\begin{array}{cc} A_{tt} & A_{tr} \\ A_{rt} & A_{rr} \end{array} \right]^{-1} \left[\begin{array}{c} 5 \\ d \end{array} \right]. \tag{2.12}
$$

223 In practice, it is more convenient to express the thermal conductivity by the Eucken factors
224 (Eucken 1913) ,

$$
225 \quad \frac{2\kappa_t}{\mu} = \frac{3}{2} f_t, \quad \frac{2\kappa_r}{\mu} = \frac{d}{2} f_r, \quad \frac{2\kappa}{\mu} = \frac{2(\kappa_t + \kappa_r)}{\mu} = \frac{3+d}{2} f_{eu}, \tag{2.13}
$$

226 where $\kappa = \kappa_t + \kappa_r$ is the overall thermal conductivity; f_{eu}, f_t and f_r are the total, translational
227 and rotational Eucken factors, respectively.

228 For the numerical solution of our kinetic equation, a boundary condition is required to
229 determine the value of f at the boundary of a computational domain. Considering a non-
230 absorbing wall with a velocity $\boldsymbol{u}_w$ at the temperature T_w, all the gas molecules $(\boldsymbol{v}', \boldsymbol{I}')$
231 hitting the wall will return to the flow field with a new state $(\boldsymbol{v}, I)$. Given the unit normal
232 vector, $\boldsymbol{n}$, of the wall pointing towards the gas, the velocity-energy distribution function of
233 the molecules in the nearest vicinity of the wall is denoted as

$$
234 \quad f_w = \left\{ \begin{array}{ll} f^-, & (\boldsymbol{v}' - \boldsymbol{u}_w) \cdot \boldsymbol{n} \leqslant 0, \\ f^+, & (\boldsymbol{v}' - \boldsymbol{u}_w) \cdot \boldsymbol{n} > 0, \end{array} \right. \tag{2.14}
$$

235 where f^- and f^+ are the distributions of the incident and reflected molecules, respectively.
236 The correlation between the incident and reflected distribution functions is defined through
237 the reflection kernel $R(\boldsymbol{v}' \rightarrow \boldsymbol{v}, I' \rightarrow I)$ as

$$
238 \quad \begin{aligned} (\boldsymbol{v} - \boldsymbol{u}_w) \cdot \boldsymbol{n} f^+(\boldsymbol{v}, I) = \\ - \iint_{(\boldsymbol{v}' - \boldsymbol{u}_w) \cdot \boldsymbol{n} \leqslant 0} (\boldsymbol{v}' - \boldsymbol{u}_w) \cdot \boldsymbol{n} f^-(\boldsymbol{v}', I') R(\boldsymbol{v}' \rightarrow \boldsymbol{v}, I' \rightarrow I) \mathrm{d}\boldsymbol{v}' \mathrm{d}I', \end{aligned} \tag{2.15}
$$

239 for all $(\boldsymbol{v}' - \boldsymbol{u}_w) \cdot \boldsymbol{n} > 0$. For a fully diffuse wall, the reflection kernel is read as

$$
240 \quad R(\boldsymbol{v}' \rightarrow \boldsymbol{v}, I' \rightarrow I) = \frac{2(\boldsymbol{v} - \boldsymbol{u}_w) \cdot \boldsymbol{n} I^{d/2-1}}{\pi \Gamma(d/2) T_w^{2+d/2}} \times \exp\left(-\frac{(\boldsymbol{v} - \boldsymbol{u}_w)^2}{T_w} - \frac{I}{T_w} \right). \tag{2.16}
$$

3. Formulation of wave propagation

242 The schematic diagram of simulation setup is exhibited in figure 1. Here, we specify the
243 formulation of wave propagation in rarefied molecular gases confined between two infinite,
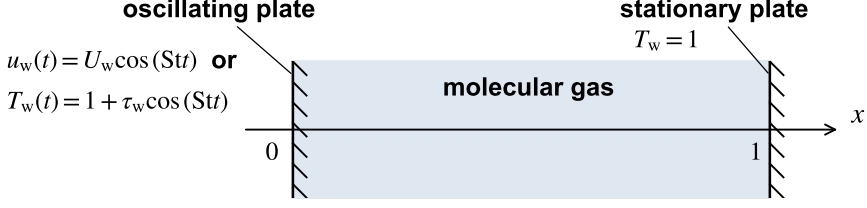
Figure 1: Schematic diagram of sound and thermal-acoustic wave propagation in rarefied molecular gases between two infinite, parallel, and impermeable plates. The oscillation plate is positioned at $x = 0$ with harmonically variant velocity (along the x-direction) or temperature, while a stationary plate is at $x = 1$. The stationary plate has a fixed temperature of $T_w = 1$. Both plates are fully diffuse walls.

244 parallel, and impermeable plates located at $x = 0$ and $x = 1$, which can be treated as a
245 simple prototype of wave propagation in confined space. The plate at $x = 0$ may oscillate
246 harmonically at a constant frequency ω in its normal direction so that the velocity varies as

$$u_w(t) = U_m \Re\{\exp(\mathrm{i}\mathrm{St}t)\}, \tag{3.1}$$

248 and a sound wave is induced in the gas. This plate may attain unsteady heating, so that its
249 temperature varies as

$$T_w(t) = 1 + \tau_m \Re\{\exp(\mathrm{i}\mathrm{St}t)\}, \tag{3.2}$$

251 and a thermal-acoustic wave is consequently induced. In eqs. (3.1) and (3.2), i is the
252 imaginary unit, $\Re\{\cdot\}$ denotes the real part of the complex expression, and U_m and τ_m
253 are the maximum speed and perturbed temperature of the plate, respectively. The constant
254 St is the normalized oscillation frequency, defined as the Strouhal number:

$$\mathrm{St} = \frac{\omega H}{v_m}. \tag{3.3}$$

256 Note that the two driving forces have the same frequency. The time-based Knudsen number
257 correlates with Kn_l and St through

$$\mathrm{Kn}_t = \frac{\mu_0 \omega}{p_0} = \frac{2\mathrm{Kn}_l \mathrm{St}}{\sqrt{\pi}}, \tag{3.4}$$

259 where p_0/μ_0 is the reference collision frequency of gas molecules.
260   We are interested in the flow state when the oscillation has been fully established. As a
261 consequence, the time-dependent behaviour of the gas is periodic with the same frequency
262 as the oscillation stimuli. We further assume that the velocity and perturbed temperature
263 of the plate are sufficiently small quantities, i.e., $u_m \ll 1$ and $\tau_m \ll 1$, hence, the gas
264 system is slightly deviated from its reference equilibrium state that is described by the global
265 Maxwellian

$$E_0 = \frac{I^{d/2-1}}{\pi^{3/2}\Gamma(d/2)}\exp\left(-|\boldsymbol{v}|^2 - I\right), \tag{3.5}$$

267 and the kinetic equations can be linearized by representing the distribution function as

$$f(t, x, \boldsymbol{v}, I) = E_0\left[1 + \Re\left\{h(x, \boldsymbol{v}, I)\exp(\mathrm{i}\mathrm{St}t)\right\}\right], \tag{3.6}$$

269 where $|h| \ll 1$ is the amplitude of the perturbed distribution function. The macroscopic flow

270 properties of interest are also expressed by the following complex functions

$$
\begin{aligned}
n(t, x) &= 1 + \Re\left\{\rho(x) \exp\left(\mathrm{i} \mathrm{St} t\right)\right\}, \\
u_x(t, x) &= \Re\left\{U(x) \exp\left(\mathrm{i} \mathrm{St} t\right)\right\}, \\
T_t(t, x) &= 1 + \Re\left\{\tau_t(x) \exp\left(\mathrm{i} \mathrm{St} t\right)\right\}, \\
T_r(t, x) &= 1 + \Re\left\{\tau_r(x) \exp\left(\mathrm{i} \mathrm{St} t\right)\right\}, \\
q_t^x(t, x) &= \Re\left\{Q_t(x) \exp\left(\mathrm{i} \mathrm{St} t\right)\right\}, \\
q_r^x(t, x) &= \Re\left\{Q_r(x) \exp\left(\mathrm{i} \mathrm{St} t\right)\right\}, \\
p_{xx}(t, x) &= 1 + \Re\left\{P(x) \exp\left(\mathrm{i} \mathrm{St} t\right)\right\},
\end{aligned}
\tag{3.7}
$$

272 where p_{xx} is the gas pressure in the direction of wave propagation. $[\rho, U, \tau_t, \tau_t, Q_t, Q_r, P]$
273 are complex quantities, which can be represented in the exponential forms as

$$
M(x) = M_{am}(x) \exp\left[\mathrm{i}\phi_M(x)\right], \quad M = \rho, U, \tau_t, \tau_r, Q_t, Q_r, P,
\tag{3.8}
$$

275 where M_{am} and ϕ are the real functions corresponding to the amplitude and phase of a
276 periodic function. Note that for the spatial coordinates, all the variables depend only on x,
277 since the propagation of wave is restricted in this direction.

278 Substituting eqs. (3.6) and (3.7) into the kinetic equation (2.1) and neglecting all the
280 nonlinear terms, we obtain the equation for h, written as

$$
\begin{aligned}
\mathrm{i} \mathrm{St} h + v_x \frac{\partial h}{\partial x} =& \delta_0 \left[\rho + 2U v_x + \tau_t \left(|\boldsymbol{v}|^2 - \frac{3}{2} \right) + \tau_r \left(I - \frac{d}{2} \right) + \right. \\
& \left. \frac{4}{15} Q_t v_x \left(|\boldsymbol{v}|^2 - \frac{5}{2} \right) + \frac{4}{d} Q_r v_x \left(I - \frac{d}{2} \right) - h \right] \\
& + \frac{\delta}{Z} \left[(\tau - \tau_t) \left(|\boldsymbol{v}|^2 - \frac{3}{2} \right) + (\tau - \tau_r) \left(I - \frac{d}{2} \right) + \right. \\
& \left. \frac{4(Q' - Q_t) \cdot \boldsymbol{v}}{15} \left(|\boldsymbol{v}|^2 - \frac{5}{2} \right) + \frac{4(Q'' - Q_r) \cdot \boldsymbol{v}}{d} \left(I - \frac{d}{2} \right) \right],
\end{aligned}
\tag{3.9}
$$

282 where $\tau = (3\tau_t + d\tau_r)/(3 + d)$, and Q' and Q'' are related to Q_t and Q_r according to
284 eq. (2.6). The boundary condition for h is

$$
\begin{aligned}
h^+ =& \sqrt{\pi} U_m - 2\sqrt{\pi} \iint_{v'_x \leqslant 0} v'_x E_0 h^- \mathrm{d}\boldsymbol{v}' \mathrm{d}I' \\
& + 2U_m v_x + \tau_m \left(|\boldsymbol{v}|^2 - \frac{5}{2} \right) + \tau_m \left(I - \frac{d}{2} \right), \quad \text{at } x = 0, \\
h^+ =& 2\sqrt{\pi} \iint_{v'_x > 0} v'_x E_0 h^- \mathrm{d}\boldsymbol{v}' \mathrm{d}I', \quad \text{at } x = 1,
\end{aligned}
\tag{3.10}
$$

286 where h^+ and h^- denote the reflected and incident perturbed distribution functions. Once h
287 is known, the macro quantities are calculated from the velocity moments as

$$
\begin{aligned}
& [\rho, U, \tau_t, \ \tau_r, Q_t, Q_r, P] = \\
& \iint \left[1, v_x, \frac{2}{3}|\boldsymbol{v}|^2 - 1, \frac{2}{d}I - 1, v_x \left(|\boldsymbol{v}|^2 - \frac{5}{2} \right), v_x \left(I - \frac{d}{2} \right), v_x^2 \right] E_0 h \mathrm{d}\boldsymbol{v} \mathrm{d}I.
\end{aligned}
\tag{3.11}
$$

289 By introducing complex expressions, the time variable in the governing equation system is
290 eliminated. The technique of computational fluid dynamics for time-independent problems is
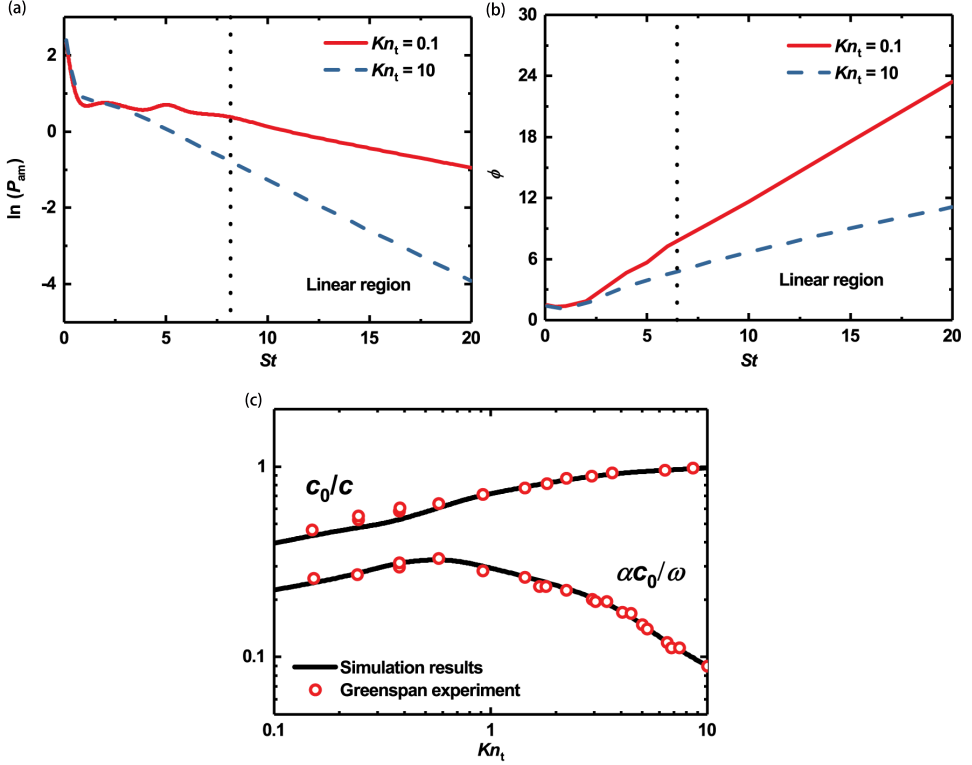291 adopted to find deterministic solutions, which can largely reduce the computational cost. The

Figure 2: Model validation: (a) variation of the pressure amplitude on the receptor with the strouhal number St; (b) phase variation on the receptor with St; (c) comparison of dimensionless sound speed and attenuation coefficient between the simulation results and the experimental data (Greenspan 1959).

292   details about the computational issues are given in the following Section and Appendix. Note
293   that this method cannot be used to simulate the propagation of a strong wave propagation
294   with large amplitude. In such a circumstance, the assumption that variant flow properties have
295   the same oscillating frequency as the external stimuli may break down, and a weak shock
296   wave may generate and propagate in space (Tang *et al.* 2001; Cox *et al.* 2001). Then, time-
297   dependent nonlinear kinetic equations should be applied to investigate such flows. Numerical
298   methods with efficient shock-capture schemes, e.g., the unified gas kinetic schemes, should
299   be used (Wang & Xu 2012; Wang *et al.* 2018).

4. Results and discussion

301   In this section, we will investigate the sound and thermoacoustic wave propagation in
302   rarefied molecular gases. A wide range of rarefactions and oscillation frequencies will
303   be considered. The influence of non-equilibrium relaxations between the translational and
304   rotational modes, in particular the bulk viscosity μ_b and the Eucken factors f_t and f_r, are to
305   be elaborated.

4.1. *Validation of kinetic model and numerical scheme*

307   As the disturbance in the gas is restrained in the x direction, dependence of the governing
308   equation system on v_y, v_z and I can be eliminated by introducing auxiliary distribution

309 functions that have independent variables x and v_x. The details of the reduced system, which
310 is to reduce computational cost, are explained in Appendix A. The kinetic equations are
311 solved by the DVM, where v_x is truncated to the range of $[-6, 6]$ and partitioned by N_v
312 non-uniformly distributed points according to

$$v_x = \frac{6}{(N_v - 1)^3}(-N_v + 1, -N_v + 3, ..., N_v - 1)^3. \tag{4.1}$$

314 In this partition, the majority of the discrete velocities are located around $v_x = 0$, conse-
315 quently, it is able to capture the discontinuity and rapid oscillation in the perturbed velocity
316 distribution function near $v_x = 0$ at the plate of $x = 0$ (Kalempa & Sharipov 2009; Wu
317 2016). We set $N_v = 80, 300$ and 300 for $Kn = 0.01, 0.1$ and 10 respectively to obtain smooth
318 solutions. The spatial domain $x \in [0, 1]$ is divided into N_x elements with refinement in the
319 vicinity of the two plates, where the boundary nodes of the elements are calculated by

$$x = s^3(10 - 15s + 6s^2), \quad s = \frac{(0, 1, ..., N_x)}{N_x}. \tag{4.2}$$

321 We set $N_x = 64$ for all the cases. The spatial derivatives are approximated by the fourth-order
322 discontinuous Galerkin method. To seek stable solutions, a semi-implicit time iterative
323 scheme is applied and the iteration stops when the residuals of density, velocity and
324 temperatures are less than 10^{-7}. The details of the numerical scheme can refer to Su
325 *et al.* (2020). The independence of the obtained results on velocity and spatial grids is
326 verified: when the discrete velocities and spatial elements are further doubled, the maximum
327 difference is not larger than 1% for the macro-quantities, such as the pressure amplitude.
328 We validate our numerical solutions by comparing them with the experimental mea-
329 surements of Greenspan (1959). In the experiment, the working gas was nitrogen, and all
330 measurements were conducted in a two-crystal interferometer. The emitting crystal was
331 fixed and energized at a constant voltage by a crystal-controlled electron-coupled oscillator,
332 generating a sound frequency of about 1MHZ. The receiving crystal was connected to a
333 movable slider while the displacement of the crystal receiver was measured. Processed
334 through the filter and amplifier, the change in gas pressure was finally obtained.
335 The rotational degree of freedom for nitrogen is $d = 2$. For numerical solutions, we
336 set the rotational collision number $Z = 2.67$ and the thermal relaxation rates $A_{tt} = 0.786$,
337 $A_{tr} = -0.201$, $A_{rt} = -0.059$, and $A_{rr} = 0.842$, thus $f_{eu} = 1.993$, $f_t = 2.365$ and $f_r = 1.435$.
338 These parameters are measured from the DSMC simulation in order to match the total thermal
339 conductivity of nitrogen at $T_0 = 300$ K obtained from the Rayleigh-Brillouin scattering (Wu
340 *et al.* 2020; Li *et al.* 2021). The numerical and experimental results are compared in terms of
341 the variations of the dimensionless attenuation coefficient α and sound speed v_{ph} against Kn_t.
342 These acoustic parameters can be expressed by the amplitude P_{am} and ϕ_P of the perturbed
343 gas pressure at $x = 1$ as

$$\alpha = -\sqrt{\frac{\gamma}{2}}\frac{\mathrm{d}\ln P_{am}}{\mathrm{dSt}}, \quad v_{ph} = \frac{c_0}{\beta}, \tag{4.3}$$

345 where $\gamma = 7/5$ is the ratio of specific heats for linear molecules, c_0 is the adiabatic sound
346 speed, and β is the dimensionless phase parameter defined as

$$\beta = \sqrt{\frac{\gamma}{2}}\frac{\mathrm{d}\phi_P}{\mathrm{dSt}}. \tag{4.4}$$

348 Numerical solutions of α and β are obtained by the point-wise method (Sharipov *et al.* 2002;
349 Garcia & Siewert 2005; Wang & Xu 2012). The P_{am} and ϕ_P can be obtained using eq. (3.8).
350 In the experiment, the Strouhal number St was controlled by adjusting the distance between

Rapids articles must not exceed this page length

351 the sound source and the receptor since the oscillation frequency was fixed. And P_{am} and
352 ϕ_P highly depend on St (Sharipov *et al.* 2002; Struchtrup 2012), see Figure 2(a) and (b).
353 When St is small, i.e., the source and the receptor are close to each other, distinctive peaks
354 and valleys appear in P_{am} due to resonance. As the distance between the plates grows, no
355 resonance is observed due to strong damping in a rarefied gas, resulting in very weak reflected
356 wave. Note that the phase ϕ_P also exhibits a non-monotonous variation when St is small.
357 Since no data were provided for the geometrical setup of the sound source and receptor in the
358 experiment, in order to eliminate the influence of resonance, $d(\ln P_{am})/dSt$ and $d\Phi_P/dSt$ in
359 eqs. (4.3) and (4.4) are determined by the linear tails of the curves in Figure 2(a) and (b).
360 Figure 2(c) shows the comparison between the simulated and measured results, from which
361 we found that our simulations can capture the essential acoustic properties of the sound wave
362 propagation in rarefied molecular gases.

4.2. *Investigation of gas damping*

364 Because of energy dissipation, gas damping occurs in sound wave propagation. In this
365 section, the change of pressure amplitude is used to describe the property of gas damping in
366 the flow channel. The gas is nitrogen, and the free parameters d, Z, and A_{ij} are the same as
367 the ones used in the previous section. Figure 3 shows the profile of pressure amplitude under
368 different Kn_l and St.

369 In a confined flow, resonance and anti-resonance will appear due to the superposition of
370 incident and reflected waves. And the intensity of resonance is determined by the reflected
371 wave as the input energy is constant. In Figure 3 (a), the collisions between particles are
372 more frequent with smaller St and Kn_l, which means more energy can be transferred to the
373 receptor, resulting in the stronger reflected wave. Consequently, the resonance is stronger as
374 well. It can be seen that the pressure amplitude at the entrance is smaller than that at the
375 receptor due to anti-resonance. With increasing Strouhal number, e.g., St = 4 in Figure 3 (b),
376 the reflected wave is weaker and the pressure amplitude at the entrance is larger than that at
377 the receptor when $Kn_l \geqslant 0.1$. In Figure 3 (c), the collisions between particles are infrequent
378 as St is large. The resonance becomes obvious when Kn is large.

379 Now we investigate the influence of bulk viscosity on gas damping. In addition to nitrogen,
380 we consider two more pseudo gases with the rotational collision number Z being 113
381 and 14250; the other parameters d and A_{ij} remain the same as those for nitrogen. Noted
382 that the choice of high Z values was made to investigate the impact of a extremely slow
383 relaxation. Previous estimation based on sound attenuation coefficients showed that certain
384 real gases, such as CO_2, may exhibit large rotational collision number and bulk viscosity
385 at low temperature (Cramer 2012). However, a recent measurement indicated the ratio of
386 the bulk and shear viscosity is about 3-5 in low-temperature CO_2 (Wang *et al.* 2019). The
387 high rotational collision number is a result of incorrect splitting of rotational and vibrational
388 modes, and the slow vibrational relaxation should be taken into account when predicting
389 the high attenuation coefficient in CO_2 (Kustova *et al.* 2023). For comparison, we also
390 simulate the sound wave propagation in a monatomic gas, which is described by the Shakhov
391 equation (Kalempa & Sharipov 2009). The profiles of pressure amplitude along the flow
392 channel are shown in Figure 4. When Kn_l and/or St are relatively large, e.g., $Kn_l = 0.1$,
393 St = 8, and $Kn_l = 10$ regardless of St, there is no difference between the simulated gases.
394 This is because the bulk viscosity exerts influence through inelastic collisions; when the
395 degree of rarefaction is high, the molecular collisions are infrequent so the pressure profiles
396 are not affected by bulk viscosities as they rely on translational energy and there is negligible
397 energy transfer between translational and rotational energies. When Kn_l and St decrease, the
398 particle collisions become more frequent so the bulk viscosity plays an important role in
399 determining the pressure amplitude. Interestingly, the pressure amplitude of a molecular gas
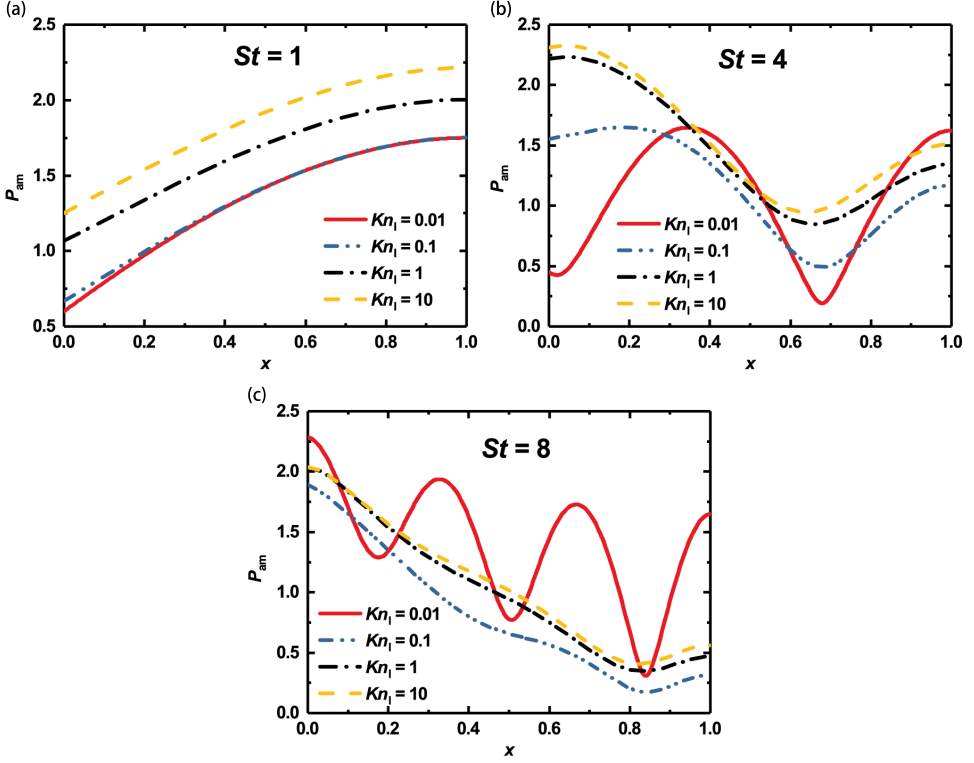
Figure 3: The change of pressure amplitude in the x direction: (a) St = 1; (b) St = 4; (c) St = 8. Kn_l is set to be 0.01, 0.1, 1 and 10, respectively.

with large bulk viscosity is very close to that of a monatomic gas under all the considered Knudsen and Strouhal numbers. This is because the internal degrees of freedom are frozen when Z is large, i.e., inelastic collisions are rare. The underlying mechanism will be further discussed in Section 4.3.

Now we turn to investigate the influence of thermal conductivity on gas damping by changing the values of translational and rotational Eucken factors. We keep the rotational collision number $Z = 2.67$, the total Eucken factor $f_{eu} = 1.993$, $A_{tr} = -0.201$ and $A_{rt} = -0.059$ the same as the experimental value of nitrogen. Figure 5 shows the pressure amplitude under various translational Eucken factors of 1.5, 2.0 and 2.5. The corresponding rotational Eucken factor and the two diagonal elements A_{tt} and A_{rr} can be obtained through Eqs. (2.12) and (2.13). Different from the bulk viscosity, the thermal conductivity exerts limited influence on gas damping over a wide range of Kn_l and St.

4.3. *Surface force on transducer*

We now evaluate the surface force on the transducer in molecular gases, which can be obtained from the gas pressure at the plate. Therefore, we will focus on the change of gas pressure amplitude at $x = 0$ under different transport coefficients and flow conditions.

The relationship between the pressure amplitude P_{am} and the Strouhal number St under different rotational collision numbers Z and Knudsen numbers Kn_l are shown in Figure 6. It is found that when Kn_l is not small, say equal to or larger than 1, the effect of particle collisions is neglected and the profiles of P_{am} remain nearly unchanged regardless of Z. Therefore, we will focus on examining the flow properties in three distinct flow regimes:
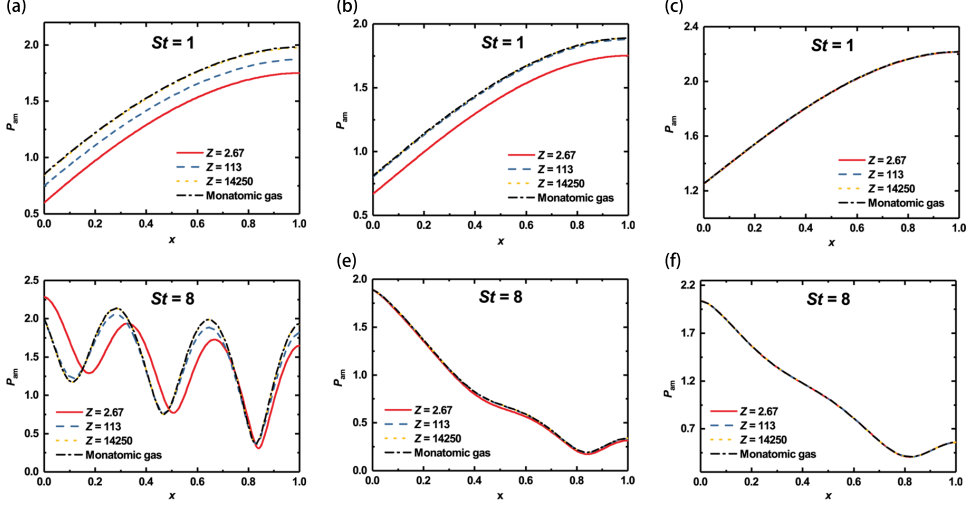
Figure 4: The change of pressure amplitude in the x direction under various rotational collision numbers. A wide range of rarefaction and oscillation frequencies are simulated: (a) $St = 1$, $Kn_l = 0.01$; (b) $St = 1$, $Kn_l = 0.1$; (c) $St = 1$, $Kn_l = 10$; (d) $St = 8$, $Kn_l = 0.01$; (e) $St = 8$, $Kn_l = 0.1$; (f) $St = 8$, $Kn_l = 10$.
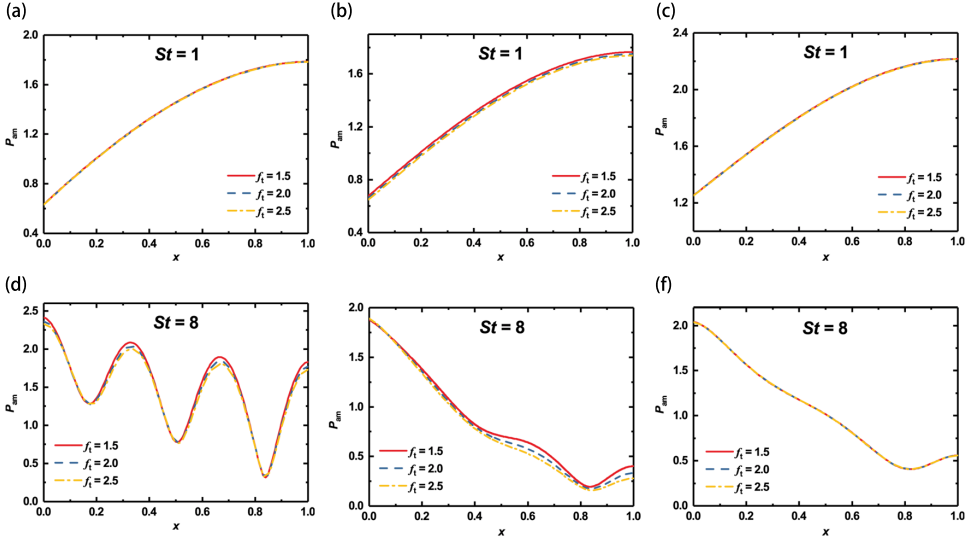

Figure 5: The change of pressure amplitude in the x direction under different translational Eucken factors. The gas is nitrogen. A wide range of rarefaction and oscillation frequencies are simulated: (a) $St = 1$, $Kn_l = 0.01$; (b) $St = 1$, $Kn_l = 0.1$; (c) $St = 1$, $Kn_l = 10$; (d) $St = 8$, $Kn_l = 0.01$; (e) $St = 8$, $Kn_l = 0.1$; (f) $St = 8$, $Kn_l = 10$.

421   $Kn_l = 0.01$, $Kn_l = 0.1$ and $Kn_l = 10$. In all the flow regimes, as St increases, P_{am} decreases
422   until the first anti-resonance frequency, and then increases to a peak value which is denoted as
423   the resonance frequency. After exceeding the first resonance frequency, P_{am} changes mildly
424   and tends to be constant when St becomes large. In order to analyze P_{am} quantitatively, we
425   first consider the case that the oscillation frequency is much larger than the mean molecular
426   collision frequency, i.e., when $Kn_l \cdot St \gg 1$. In this case, the collision term in Eq. (3.9) can be
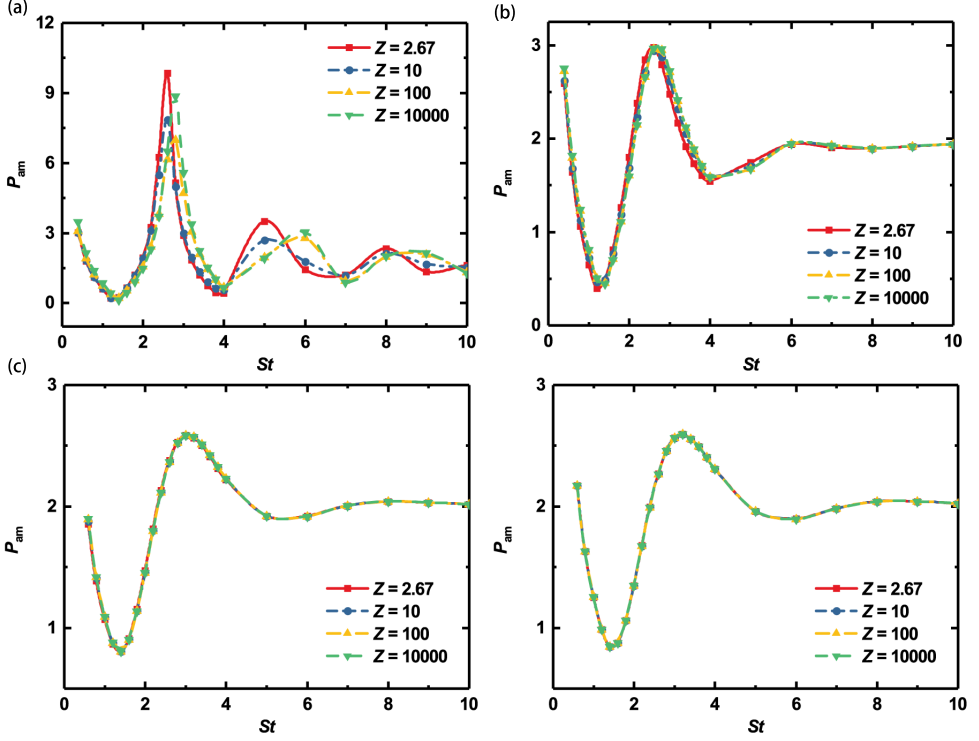
Figure 6: The relationship between pressure amplitude and St under different rotational collision numbers. The results of four flow regimes are shown here: (a) $Kn_l = 0.01$, (b) $Kn_l = 0.1$, (c) $Kn_l = 1$ and (d) $Kn_l = 10$. The rotational collision number Z is set as 2.67, 10, 100, 10000, respectively.

neglected (Kalempa & Sharipov 2009; Wu 2016). Therefore, we obtain the reduced equation

$$i \mathrm{St} h + v_x \frac{\partial h}{\partial x} = 0. \tag{4.5}$$

Combining with the boundary condition on the left plate, we can finally obtain the value of pressure amplitude on the transducer ($x = 0$) at the high-frequency limit as

$$P_{am}(x = 0) \rightarrow \frac{2}{\sqrt{\pi}} + \frac{\sqrt{\pi}}{2} \approx 2. \tag{4.6}$$

In figure 6(b) and (d), when the frequency is large, e.g., St is larger than 6, P_{am} approaches 2. However, when Kn_l is 0.01 (see Figure 6(a)), P_{am} is slightly less than 2 at large Strouhal numbers due to the fact the particle collisions are frequent and cannot be neglected.

Now, we examine the anti-resonance and resonance frequencies. Through the confined flow channel, the molecules leave the left plate with velocity v_p, reflected by the right plate, and finally return to the left plate. Without collision, the total travel distance for a molecule in the x direction is $2H$. Thus, we obtain the following equation,

$$2H \approx v_p \cdot \delta t, \tag{4.7}$$

where δt is the travelling time of each molecule. When the travelling time satisfies

$$\delta t = \frac{2n\pi}{\omega}, \quad \text{or} \quad \frac{(2n-1)\pi}{\omega}, \quad n \in N_+, \tag{4.8}$$

442 the molecules leaving and coming back to the left plate have the same or opposite phase,
443 corresponding to the resonance or anti-resonance point. Replacing ω by St, we finally obtain
444 the resonance frequency St_r and anti-resonance frequency St_a as

$$St_r \approx \frac{v_p}{v_m} n\pi, \quad n \in N_+, \tag{4.9}$$

$$St_a \approx \frac{v_p}{v_m} \frac{(2n-1)\pi}{2}, \quad n \in N_+. \tag{4.10}$$

448 For free molecular flow ($Kn_l = 10$), the collisions between particles can be neglected and
449 the travelling distance of molecules in the x direction is $2H$. In addition, the gas flow slightly
450 deviates from the global equilibrium state, thus $v_p \approx v_m$. Then, we obtain the first resonance
451 frequency $St_r \approx \pi \approx 3.14$ and the first anti-resonance frequency $St_a \approx \pi/2 \approx 1.57$ through
452 eqs. (4.9) and (4.10) which are consistent with the results shown in Figure 6(d). When
453 $Kn_l = 0.1$ and $Kn_l = 0.01$, the increased frequency of collisions makes the free movement
454 of molecules more difficult. So the real travelling time of particles is larger than $2H/v_p$.
455 Therefore, the first resonance frequency and anti-resonance frequency are smaller than the
456 respective theoretical values.

457   The influence of the bulk viscosity on the pressure amplitude at $x = 0$ is also investigated.
458 As shown in Figure 6, the bulk viscosity only affects the pressure amplitude in the slip regime
459 ($Kn_l = 0.01$). In the transition and free molecular flow regimes ($Kn_l = 0.1$ and $Kn_l = 10$),
460 due to infrequent particle collisions, the bulk viscosity exerts limited influence on P_{am}.
461 Therefore, we will focus only on the slip flow regime. From Figure 6(a), it is found that
462 the value of P_{am} varies at a fixed St for different bulk viscosities. To reveal the underlying
463 physics, we further plot the profile of P_{am} under different rotational collision numbers with
464 different St numbers, see Figure 7(a). It can be seen that, with increasing Z, P_{am} is first
465 found to monotonically converge to the constant value of a corresponding monatomic gas
466 (i.e. the dotted line in Figure 7(a)). The result indicates that the internal degrees of freedom
467 will be frozen for large bulk viscosity because of negligible inelastic collisions as we have
468 discussed in Section 4.2. We now further explain this phenomenon here. There is only one
469 inelastic collision in a total of Z collisions, which transfers the energy between translational
470 and internal energies. When Z is large, the inelastic collision frequency is low and then
471 internal energy transfer can be ignored within the characteristic time of the flow field, so
472 the pressure amplitude of molecular gases is equal to that of the corresponding monatomic
473 gases. This is called the frozen state or the local thermodynamics equilibrium (Jaeger *et al.*
474 2018).

475   In order to provide more evidence, we plot the change of perturbed temperature under
476 different Z with $St = 6.0$. As shown in Figure 7(b), the perturbed rotational temperature τ_r
477 decreases continuously with the increase of Z due to the decrease of inelastic collision. And
478 when the rotational collision number is large, e.g., more than 1000, the perturbed rotational
479 temperature is close to zero. Consequently, the perturbed overall temperature is reduced to
480 $\tau \approx 0.6\tau_t$ for molecular gases ($d = 2$) as expected theoretically.

481   Figure 6(a) shows that the bulk viscosity also influences the resonance frequency.
482 Specifically, the emerge of resonance frequency will be delayed under large bulk viscosity and
483 this trend is more obvious when St is large. As previously mentioned, when the value of Z is
484 reduced, inelastic collisions become more frequent. Such collisions result in higher rotational
485 energy and lower translational energy of the gas molecules in sound wave propogation. And
486 this causes an increase in travel time. Consequently, the resonance frequencies decrease when
487 the bulk viscosity decreases. For instance, when $Z = 2.67, 10$, the first resonance frequencies
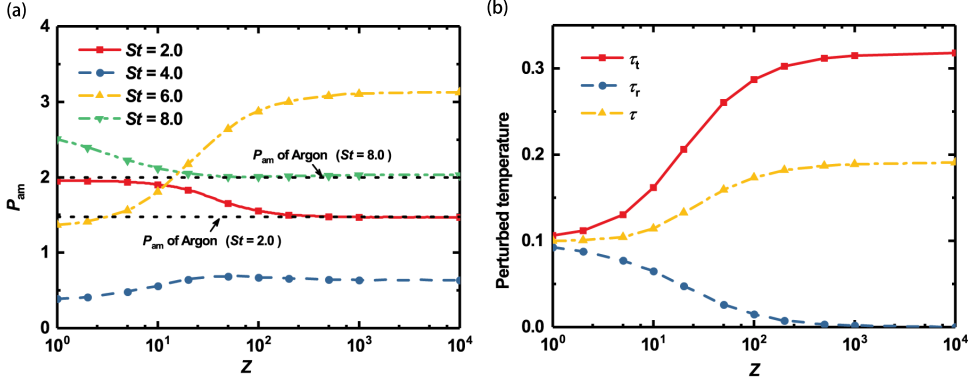488 are slightly smaller than those of $Z = 100, 10000$. In addition to that, since the resonance

Figure 7: (a) The change of pressure amplitude under different rotational collision numbers with $St = 2.0, 4.0, 6.0, 8.0$, where two dotted lines denote argon at $St = 2.0$ and $St = 8.0$; (b) amplitude of translational, rotational and total temperatures for different rotational collision numbers with $St = 6.0$;

state varies with bulk viscosity, the initial variation of P_{am} depends on St as shown in Figure 7(a).

The influence of thermal conductivity on the surface force is also investigated. The total Eucken factor is fixed as $f_{eu} = 1.993$ while the value of f_t is varied. As shown in Figure 8, the Eucken factor has little influence on the pressure amplitude and the resonance frequency.

5. Onsager-Casimir reciprocal relationship

In this section, we examine whether Onsager-Casimir reciprocal relationship (OCRR) also holds for molecular gases. If we consider a weakly non-equilibrium system where some irreversible processes occur, then the corresponding physical law can be described in a general linear form as

$$J_k = \sum_n \Lambda_{kn} X_n, \tag{5.1}$$

where X_n are driven forces, J_k are conjugated thermodynamic fluxes and Λ_{kn} is the matrix of kinetic coefficients. The non-diagonal elements Λ_{kn} $(k \neq n)$ contain both solutions corresponding to the forces X_k and X_n. If the set of the thermodynamic flow J_k is chosen so that the entropy production s in the statistical system is expressed as

$$s = \sum_k J_k X_k, \tag{5.2}$$

then the kinetic coefficients satisfy

$$\Lambda_{kn}^t = \Lambda_{nk}^t, \tag{5.3}$$

where the superscript t means that each coefficient Λ_{kn}, composed of two solutions k and n, is calculated from the time-reverted molecular state of one of these solutions.

From the Boltzmann equation, the thermodynamic fluxes and forces can be identified for gas flows, and the kinetic coefficients are derived as (Sharipov 2006)

$$\Lambda_{kn} = \int_\Sigma \left(\boldsymbol{v} \cdot \boldsymbol{n} h_w^{(k)}, h^{(n)} - \frac{1}{2} h_w^{(n)} \right) d\Sigma - i St \left(\left(h^{(k)}, h^{(n)} \right) \right), \tag{5.4}$$
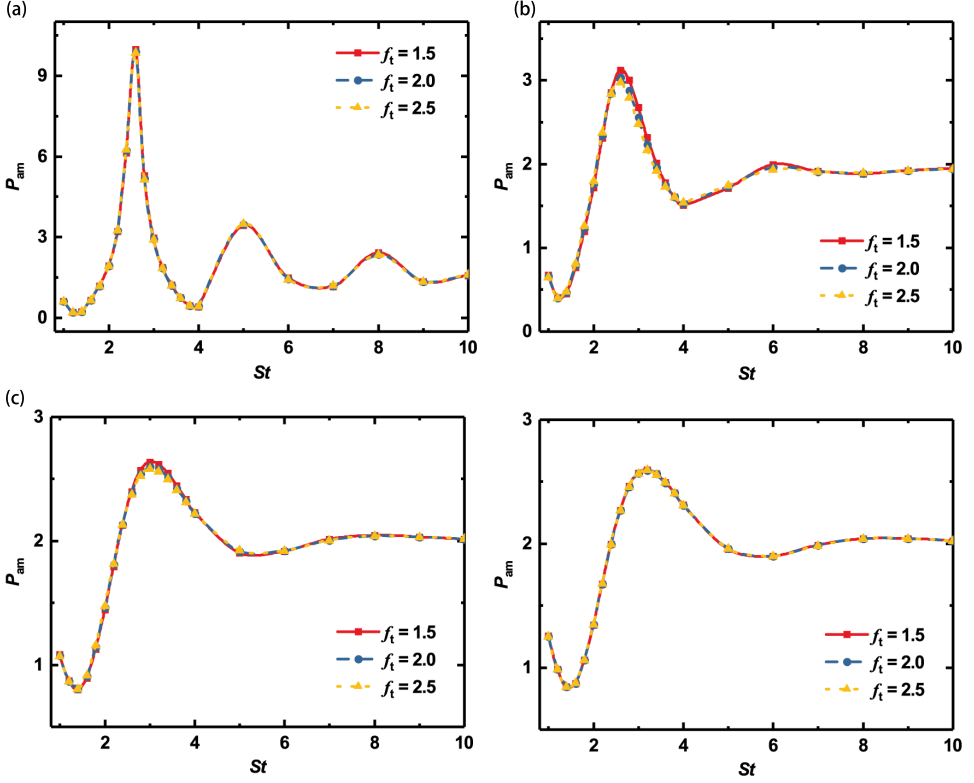
Figure 8: The relationship between pressure amplitude and *St* under different translational Eucken factors. Four flow regimes are investigated:(a) $Kn_l = 0.01$; (b) $Kn_l = 0.1$; (c) $Kn_l = 1$ and (d) $Kn_l = 10$. The translational Eucken factor f_t is set to be 1.5, 2, 2.5, respectively.

$$\Lambda^t_{kn} = \int_\Sigma \left(\mathcal{T} \boldsymbol{v} \cdot \boldsymbol{n} h_w^{(k)}, h^{(n)} - \frac{1}{2} h_w^{(n)} \right) d\Sigma - i \text{St} \left(\left(\mathcal{T} h^{(k)}, h^{(n)} \right) \right), \tag{5.5}$$

where Σ represents solid walls that enclose the flow field Ω; h_w is given by the wall velocity and temperature as

$$h_w = 2\boldsymbol{v} \cdot \boldsymbol{u}_w + \tau_w \left(|\boldsymbol{v}|^2 - \frac{5}{2} \right) + \tau_w \left(I - \frac{d}{2} \right); \tag{5.6}$$

and the binary operations $(\cdot, \cdot)$ and $((\cdot, \cdot))$ are defined for the two arbitrary functions as

$$(\phi, \psi) = \iint E_0 \phi(\boldsymbol{x}, \boldsymbol{v}, I) \psi(\boldsymbol{x}, \boldsymbol{v}, I) d\boldsymbol{v} dI, \tag{5.7}$$

$$((\phi, \psi)) = \int_\Omega (\phi, \psi) \, d\boldsymbol{x}. \tag{5.8}$$

Finally, $\mathcal{T}$ is the operator reversing the state of molecules in time

$$\mathcal{T} \phi(\boldsymbol{x}, \boldsymbol{v}, I) = \phi(\boldsymbol{x}, \boldsymbol{v}^t, I^t), \tag{5.9}$$

which is self-conjugated, i.e.,

$$(\mathcal{T} \phi, \psi) = (\mathcal{T} \psi, \phi). \tag{5.10}$$

525 For the sound wave stimulated by oscillation of the transducer and the thermoacoustic
526 wave induced by a temperature oscillation, the thermodynamic forces are defined as

$$X_U = u_m, \quad X_T = \tau_m, \tag{5.11}$$

528 then the perturbed distribution can be expressed as

$$h(x, \boldsymbol{v}, I) = h^{(U)}(x, \boldsymbol{v}, I) X_U + h^{(T)}(x, \boldsymbol{v}, I) X_T. \tag{5.12}$$

530 And h_w that defines the boundary condition can also be decomposed as

$$h_w(x, \boldsymbol{v}, I) = h_w^{(U)}(x, \boldsymbol{v}, I) X_U + h_w^{(T)}(x, \boldsymbol{v}, I) X_T, \tag{5.13}$$

532 where

$$h_w^{(U)} = \begin{cases} 2v_x, & x = 0, \\ 0, & x = 1, \end{cases} \tag{5.14}$$

$$h_w^{(T)} = \begin{cases} \left(|\boldsymbol{v}|^2 - \frac{5}{2}\right) + \left(I - \frac{d}{2}\right), & x = 0, \\ 0, & x = 1. \end{cases} \tag{5.15}$$

536 Using the reciprocal relation, i.e., eq. (5.1), the kinetic coefficients given by eqs. (5.4) and
538 (5.5), and the self-conjugated property described by eq. (5.10), we obtain

$$\left(\mathcal{T} v_x h_w^{(U)}, h^{(T)}\right)_{x=0} - \left(\mathcal{T} v_x h_w^{(U)}, h^{(T)}\right)_{x=1} = \left(\mathcal{T} v_x h_w^{(T)}, h^{(U)}\right)_{x=0} - \left(\mathcal{T} v_x h_w^{(T)}, h^{(U)}\right)_{x=1}$$
$$+ \left(\mathcal{T} v_x h_w^{(U)}, h_w^{(T)}\right)_{x=0} - \left(\mathcal{T} v_x h_w^{(U)}, h_w^{(T)}\right)_{x=1}. \tag{5.16}$$

541 Inserting $h_w^{(U)}$ and h_w^T, we have

$$\left(\mathcal{T} 2|\boldsymbol{v}|^2, h^{(T)}\right)_{x=0} = \left(\mathcal{T} v_x (|\boldsymbol{v}|^2 - \frac{5}{2}), h^{(U)}\right)_{x=0} + \left(\mathcal{T} v_x (I - \frac{d}{2}), h^{(U)}\right)_{x=0}$$
$$+ \left(\mathcal{T} 2|\boldsymbol{v}|^2, (|\boldsymbol{v}|^2 - \frac{5}{2})\right)_{x=0} + \left(\mathcal{T} 2|\boldsymbol{v}|^2, (I - \frac{d}{2})\right)_{x=0}, \tag{5.17}$$

543 thus

$$P^{(T)} = -Q_t^{(U)} - Q_r^{(U)} = -Q^{(U)}, x = 0. \tag{5.18}$$

545 If we use $h^{(T)}(1 - x, \boldsymbol{v}, I)$ instead of $h^{(T)}(x, \boldsymbol{v}, I)$, the boundary condition is then
546 transformed as

$$h_w^{(T)}(1 - x) = \begin{cases} 0, & x = 0, \\ \left(|\boldsymbol{v}|^2 - \frac{5}{2}\right) + \left(I - \frac{d}{2}\right), & x = 1. \end{cases} \tag{5.19}$$

548 The reciprocal relation gives

$$\left(\mathcal{T} 2|\boldsymbol{v}|^2, h^{(T)}(1 - x)\right)_{x=0} = -\left(\mathcal{T} v_X (|\boldsymbol{v}|^2 - \frac{5}{2}), h^{(U)}(x)\right)_{x=1} - \left(\mathcal{T} v_X (I - \frac{d}{2}), h^{(U)}(x)\right)_{x=1}, \tag{5.20}$$

550 thus

$$P^{(T)} = Q_t^{(U)} + Q_r^{(U)} = Q^{(U)}, \; x = 1. \tag{5.21}$$

552 Therefore, OCRR for the wave propagation in molecular gases is confirmed by Eqs. (5.18)
553 and (5.21), which show that the magnitude of the deviation of gas pressure at the walls
554 induced by the thermoacoustic wave is equal to the magnitude of the total heat flux (sum of
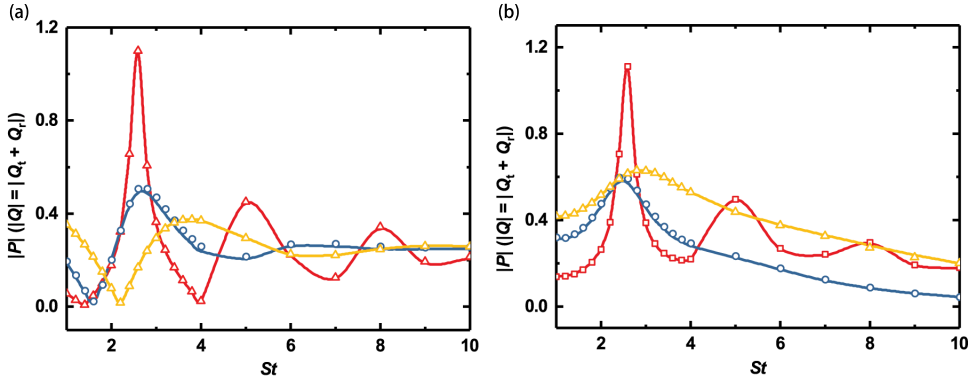555 the translational and internal heat fluxes) induced by the sound wave.

Figure 9: The variation of pressure amplitude and heat flux under different *St*: (a) $x = 0$ and (b) $x = 1$. The solid lines denote the pressure amplitude while the hollow points represent the heat flux. Three colors denote different flow regimes while red represents the slip regime ($Kn_l = 0.01$), blue, the transition regime ($Kn_l = 0.1$), and yellow, the free molecular flow regime ($Kn_l = 10$).

We further show the numerical results of the pressure amplitude and the total heat flux under a wide range of St and Kn_l. The results on the transducer and receptor are shown in Figure 9. In all the flow regimes, the pressure amplitude in the thermoacoustic wave agrees with the heat flux in the sound wave, suggesting that OCRR also holds for molecular gases.

The comparison between the pressure amplitude of the thermoacoustic wave and the total heat flux of the sound wave under different bulk viscosity and thermal conductivity is shown in Figure 10. The simulation is conducted in the slip regime with $Kn = 0.01$. It is evident that OCRR is valid under different values of bulk viscosity and thermal conductivity. From the left column of Figure 10, we can see the influence of bulk viscosity and thermal conductivity on the thermoacoustic wave. In Figure 10(a), the resonance frequency is shifted when the bulk viscosity is altered, which is similar to the behavior of the sound wave. The only difference lies in the value of P_{am}. In the case of the thermoacoustic wave, the pressure variation is generated by the oscillation of temperature, resulting in a significantly lower pressure amplitude than that in the sound wave. Figure 10(c, d) shows that thermal conductivity has little influence on the pressure amplitude of the thermoacoustic wave and the heat flux amplitude of the sound wave.

6. Conclusions

We have investigated the sound wave propagation in rarefied molecular gases over a wide range of rarefactions and oscillation frequencies. We first evaluate the influence of the transport coefficients on gas damping, and find that both rarefaction and oscillation frequency affect the pressure amplitude and resonance/anti-resonance of the sound wave. As for the transport coefficients, bulk viscosity only exerts influence on the pressure amplitude at small Kn_l and St. At larger Kn_l and St, the pressure amplitude is not affected by bulk viscosity. The pressure amplitude converges to the value of the corresponding monatomic gas when the bulk viscosity increases. Our results show that the internal degrees of freedom are frozen at large bulk viscosity, so rotational mode has little influence and the results are similar to a monatomic gas. Meanwhile, thermal conductivity has a limited effect on the pressure amplitude and the total heat flux of the sound wave.

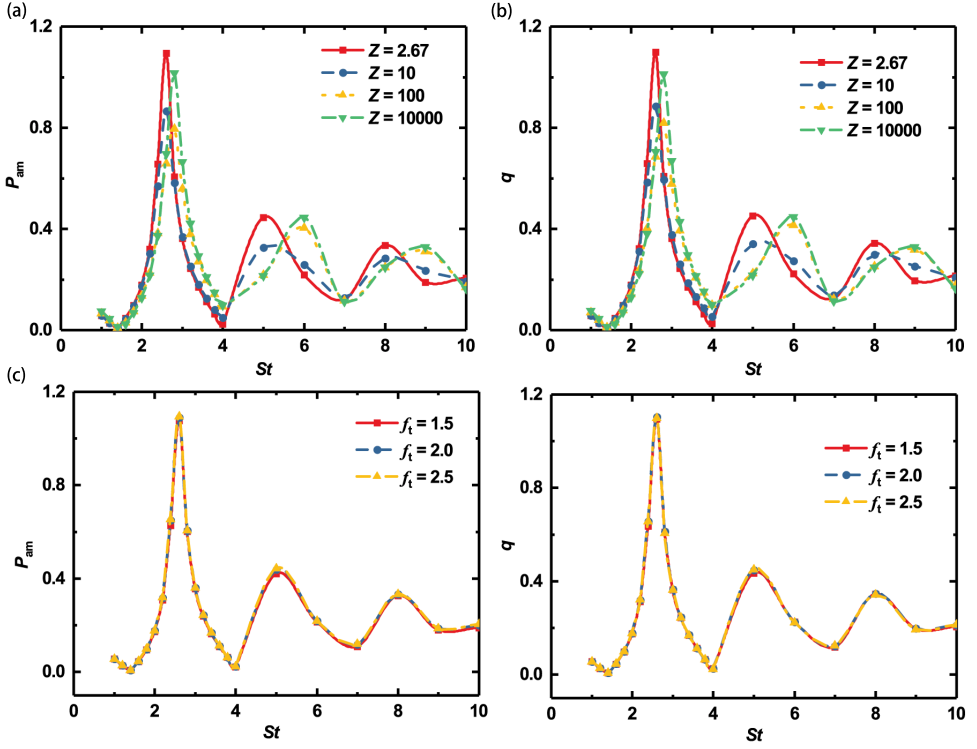The propagation of thermoacoustic waves has also been investigated. We have proved,

Figure 10: The comparison between the pressure amplitude of the thermoacoustic wave and the total heat flux of the sound wave under different bulk viscosity and thermal conductivity. The pressure amplitude of the thermoacoustic wave is shown in the left column while the total heat flux of the sound wave is shown in the right column.

both analytically and numerically, that the Onsager-Casimir reciprocal relationship holds for molecular gases.

Declaration of interests. The authors report no conflict of interest.

Data availability statement. The data that support the findings of this study are openly available in [repository name] at http://doi.org/[doi], reference number [reference number].

Author ORCID. Y.Z., https://orcid.org/0000-0002-0683-7050

Appendix A. Derivation of the one-dimensional kinetic model

To reduce the computational cost, we first eliminate the dependency of h on the rotational energy I by introducing the following two reduced distribution functions

$$h_0 = \int E_r^0 h \mathrm{d}I, \quad h_1 = \int E_r^0 I h \mathrm{d}I \qquad (A\,1)$$

600 and further introduce

$$h_2 = h_1 - \frac{d}{2}h_0, \tag{A 2}$$

602 where the equilibrium distribution function E_r^0 can be expressed by

$$E_r^0 = \frac{I^{d/2-1}}{\Gamma(d/2)}\exp(-I). \tag{A 3}$$

605 The governing equations eventually become

$$iSth_0 + v_x\frac{\partial h_0}{\partial x} = \delta\left[\rho + 2Uv_x + \tau_t\left(|\boldsymbol{v}|^2 - \frac{3}{2}\right) + \frac{4}{15}Q_tv_x\left(|\boldsymbol{v}|^2 - \frac{5}{2}\right) - h_0\right]$$
$$+ \frac{\delta}{Z}\left[(\tau - \tau_t)\left(|\boldsymbol{v}|^2 - \frac{3}{2}\right) + \frac{4(Q' - Q_t)v_x}{15}\left(|\boldsymbol{v}|^2 - \frac{5}{2}\right)\right] \tag{A 4}$$

$$h_2 + v_x\frac{\partial h_2}{\partial x} = \delta\left[\frac{d}{2}\tau_r - h_2\right] + \frac{d\delta}{2Z}(\tau - \tau_r) + \frac{2\delta}{Z}Q'''v_x, \tag{A 5}$$

608 where

$$Q''' = -A_{rt}ZQ_t + Z(1 - A_{rr})Q_r. \tag{A 6}$$

610 The macroscopic quantities are calculated from h_0 and h_2 as

$$[\rho, U, \tau_t, Q_t] = \int\left[1, v_x, \frac{2}{3}|\boldsymbol{v}|^2 - 1, v_x\left(|\boldsymbol{v}|^2 - \frac{5}{2}\right)\right]E_t^0 h_0 \mathrm{d}\boldsymbol{v}. \tag{A 7}$$

$$[\tau_r, Q_r] = \int\left[\frac{2}{d}, v_x\right]E_t^0 h_2 \mathrm{d}\boldsymbol{v}. \tag{A 8}$$

614 Now we cast the governing equations from the three-dimensional velocity space to the
615 one-dimensional velocity space by introducing the following reduced distributions

$$\Phi_0(x, v_x) = \frac{1}{\pi}\int\exp(-v_y^2 - v_z^2)h_0 \mathrm{d}v_y \mathrm{d}v_z, \tag{A 9}$$

$$\Phi_1(x, v_x) = \frac{1}{\pi}\int\exp(-v_y^2 - v_z^2)\left(v_y^2 + v_z^2 - 1\right)h_0 \mathrm{d}v_y \mathrm{d}v_z, \tag{A 10}$$

$$\Psi(x, v_x) = \frac{1}{\pi}\int\exp(-v_y^2 - v_z^2)h_2 \mathrm{d}v_y \mathrm{d}v_z. \tag{A 11}$$

622 Then the governing equations become

$$iSt\Phi_0 + v_x\frac{\partial \Phi_0}{\partial x} = \delta\left[\rho + 2Uv_x + \tau_t\left(v_x^2 - \frac{1}{2}\right) + \frac{4}{15}Q_tv_x\left(v_x^2 - \frac{3}{2}\right) - \Phi_0\right]$$
$$+ \frac{\delta}{Z}\left[(\tau - \tau_t)\left(v_x^2 - \frac{1}{2}\right) + \frac{4(Q' - Q_t)v_x}{15}\left(v_x^2 - \frac{3}{2}\right)\right] \tag{A 12}$$

$$iSt\Phi_1 + v_x\frac{\partial \Phi_1}{\partial x} = \delta\left[\tau_t + \frac{4}{15}Q_tv_x - \Phi_1\right] + \frac{\delta}{Z}\left[(\tau - \tau_t) + \frac{4(Q' - Q_t)v_x}{15}\right], \tag{A 13}$$

$$\Psi + v_x\frac{\partial \Psi}{\partial x} = \delta\left[\frac{d}{2}\tau_r - \Psi\right] + \frac{d\delta}{2Z}(\tau - \tau_r) + \frac{2\delta}{Z}Q'''v_x. \tag{A 14}$$

626 The full diffuse boundary conditions for Φ_0, Φ_1 and Ψ can be obtained by

22

$$\Phi_0(x = 0, v_x > 0) = \sqrt{\pi} U_m - 2\sqrt{\pi} \int_{v_x \leqslant 0} v_x E_t^{01} \Phi_0 dv_x + 2U_m v_x + \tau_m(v_x^2 - 1), \quad \text{(A 15)}$$

$$\Phi_0(x = 1, v_x < 0) = \sqrt{\pi} U_m + 2\sqrt{\pi} \int_{v_x \geqslant 0} v_x E_t^{01} \Phi_0 dv_x + 2U_m v_x + \tau_m(v_x^2 - 1), \quad \text{(A 16)}$$

$$\Phi_1(x = 1, v_x < 0) = \Phi_1(x = 1, v_x > 0) = \tau_w(v_x^2 - \frac{3}{2}), \quad \text{(A 17)}$$

$$\Psi(x = 1, v_x < 0) = \Psi(x = 1, v_x > 0) = \frac{d}{2}\tau_w, \quad \text{(A 18)}$$

with the equilibrium distribution function

$$E_t^{01} = \frac{1}{\sqrt{\pi}}\exp(-v_x^2). \quad \text{(A 19)}$$

The macroscopic quantities can be calculated by

$$[\rho, U, \tau_t, Q_t] = \int \left[1, v_x, \frac{2}{3}(v_x^2 - \frac{1}{2}), v_x\left(v_x^2 - \frac{3}{2}\right)\right] E_t^{01}\Phi_0 dv_x + \int \left[0, 0, \frac{2}{3}, v_x\right] E_t^{01}\Phi_1 dv_x, \quad \text{(A 20)}$$

$$[\tau_r, Q_r] = \int \left[\frac{2}{d}, v_x\right] E_t^{01}\Psi dv_x. \quad \text{(A 21)}$$

REFERENCES

ARIMA, T., RUGGERI, T. & SUGIYAMA, M. 2017 Rational extended thermodynamics of a rarefied polyatomic gas with molecular relaxation processes. *Phys. Rev. E* **96** (4), 042143.

BIRD, G. A. 1994 *Molecular Gas Dynamics and the Direct Simulation of Gas Flows*. Clarendon Press, Oxford.

BISI, M. & LORENZANI, S. 2016 High-frequency sound wave propagation in binary gas mixtures flowing through microchannels. *Phys. Fluids* **28** (5), 052003.

BOOM, B. A., BERTOLINI, A., HENNES, E. & VAN DEN BRAND, J. F. 2021 Gas damping in capacitive MEMS transducers in the free molecular flow regime. *Sensors* **21** (7), 2566.

BORGNAKKE, CLAUS & LARSEN, POUL S. 1975 Statistical collision model for Monte Carlo simulation of polyatomic gas mixture. *Journal of Computational Physics* **18** (4), 405–420.

CASIMIR, H. B. G. 1945 On Onsager's principle of microscopic reversibility. *Rev. Mod. Phys.* **17** (2-3), 343.

CHIGULLAPALLI, S., WEAVER, A. & ALEXEENKO, A. 2012 Nonlinear effects in squeeze-film gas damping on microbeams. *J. Micromech. Microeng.* **22** (6), 065010.

CLARK, J. R., HSU, W. T., ABDELMONEUM, M. A. & NGUYEN, C. C. 2005 High-Q UHF micromechanical radial-contour mode disk resonators. *J. Microelectromech. Syst.* **14** (6), 1298–1310.

COX, E. A., MORTELL, M. P. & RECK, S. 2001 Nonlinear standing and resonantly forced oscillations in a tube with slowly changing length. *SIAM Journal on Applied Mathematics* **62** (3), 965–989.

CRAMER, M. S. 2012 Numerical estimates for the bulk viscosity of ideal gases. *Phys. Fluids* **24** (6).

DAIN, Y. & LUEPTOW, R. M. 2001a Acoustic attenuation in a three-gas mixture: Results. *J. Acoust. Soc. Am.* **110** (6), 2974–2979.

DAIN, Y. & LUEPTOW, R. M. 2001b Acoustic attenuation in three-component gas mixtures—Theory. *J. Acoust. Soc. Am.* **109** (5), 1955–1964.

DESVILLETTES, L. & LORENZANI, S. 2012 Sound wave resonances in micro-electro-mechanical systems devices vibrating at high frequencies according to the kinetic theory of gases. *Phys. Fluids* **24** (9), 092001.

EJAKOV, S. G., PHILLIPS, S., DAIN, Y., LUEPTOW, R. M. & VISSER, J. H. 2003 Acoustic attenuation in gas mixtures with nitrogen: Experimental data and calculations. *J. Acoust. Soc. Am.* **113** (4), 1871–1879.

EMERSON, DAVID R., GU, XIAO-JUN, STEFANOV, STEFAN K., YUHONG, SUN & BARBER, ROBERT W. 2007 Nonplanar oscillatory shear flow: From the continuum to the free-molecular regime. *Physics of Fluids* **19** (10), 107105, arXiv: https://pubs.aip.org/aip/pof/article-pdf/doi/10.1063/1.2799203/15813575/107105_1_online.pdf.

EUCKEN, A. 1913 Über das wärmeleitvermögen, die spezifische wärme und die innere reibung der gase. *Phys. Z* **14** (8), 324–332.

FRANGI, A., FREZZOTTI, A. & LORENZANI, S. 2007 On the application of the BGK kinetic model to the analysis of gas-structure interactions in MEMS. *Comput. Struct.* **85** (11-14), 810–817.

GARCIA, R. D. M. & SIEWERT, C. E. 2005 The linearized Boltzmann equation: Sound-wave propagation in a rarefied gas. *Z. fur Angew. Math. Phys.* **57** (1), 94–122.

GORJI, M. H. & JENNY, P. 2013 A Fokker–Planck based kinetic model for diatomic rarefied gas flows. *Phys. Fluids* **25** (6), 062002.

GREENSPAN, M. 1959 Rotational relaxation in nitrogen, oxygen, and air. *J. Acoust. Soc. Am.* **31** (2), 155–160.

HADJICONSTANTINOU, NICOLAS G. 2002 Sound wave propagation in transition-regime micro- and nanochannels. *Physics of Fluids* **14** (2), 802–809, arXiv: https://pubs.aip.org/aip/pof/article-pdf/14/2/802/12346228/802_1_online.pdf.

HOLWAY, J. & LOWELL, H. 1966 New statistical models for kinetic theory: methods of construction. *Phys. Fluids* **9** (9), 1658–1673.

IVANOV, M. S. & ROGASINSKII, S. V. 1991 Theoretical analysis of traditional and modern schemes of the DSMC method. In *Rarefied Gas Dynamics*, pp. 629–642.

JAEGER, F., MATAR, O. K. & MÜLLER, E. A. 2018 Bulk viscosity of molecular fluids. *J. Chem. Phys.* **148** (17), 174504.

KALEMPA, D. & SHARIPOV, F. 2009 Sound propagation through a rarefied gas confined between source and receptor at arbitrary Knudsen number and sound frequency. *Phys. Fluids* **21** (10), 103601.

KALEMPA, D. & SHARIPOV, F. 2012 Sound propagation through a rarefied gas. Influence of the gas–surface interaction. *Int. J. Heat Fluid Flow* **38**, 190–199.

KALEMPA, D. & SHARIPOV, F. 2014 Numerical modelling of thermoacoustic waves in a rarefied gas confined between coaxial cylinders. *Vacuum* **109**, 326–332.

KOSUGE, S. & AOKI, K. 2018 Shock-wave structure for a polyatomic gas with large bulk viscosity. *Phys. Rev. Fluids* **3** (2), 023401.

KREMER, G. M., KUNOVA, O. V., KUSTOVA, E. V. & OBLAPENKO, G. P. 2018 The influence of vibrational state-resolved transport coefficients on the wave propagation in diatomic gases. *Phys. A* **490**, 92–113.

KUSTOVA, E., MEKHONOSHINA, M., BECHINA, A., LAGUTIN, S. & VOROSHILOVA, Y. 2023 Continuum models for bulk viscosity and relaxation in polyatomic gases. *Fluids* **8** (2), 48.

LI, QI, ZENG, JIANAN, HUANG, ZEMIN & WU, LEI 2023 Kinetic modelling of rarefied gas flows with radiation. *Journal of Fluid Mechanics* **965**, A13.

LI, Q., ZENG, J., SU, W. & WU, L. 2021 Uncertainty quantification in rarefied dynamics of molecular gas: rate effect of thermal relaxation. *J. Fluid Mech.* **917**, A58.

MANDELSHTAM, L. I. & LEONTOVICH, M. A. 1937 A theory of sound absorption in liquids. *J. Exp. Theor. Phys* **7** (3), 438–449.

MASON, E. A. & MONCHICK, L. 1962 Heat conductivity of polyatomic and polar gases. *J. Chem. Phys.* **36** (6), 1622–1639.

MCCORMACK, F. J. 1968 Kinetic equations for polyatomic gases: the 17-moment approximation. *Phys. Fluids* **11** (12), 2533–2543.

MORSE, T. F. 1964 Kinetic model for gases with internal degrees of freedom. *Phys. Fluids* **7** (2), 159–169.

ONSAGER, L. 1931a Reciprocal relations in irreversible processes. i. *Phys. Rev.* **37** (4), 405.

ONSAGER, L. 1931b Reciprocal relations in irreversible processes. ii. *Phys. Rev.* **38** (12), 2265.

PARK, J. H., BAHUKUDUMBI, P. & BESKOK, A. 2004 Rarefaction effects on shear driven oscillatory gas flows: A direct simulation Monte Carlo study in the entire Knudsen regime. *Phys. Fluids* **16** (2), 317–330.

RAHIMI, B. & STRUCHTRUP, H. 2014 Capturing non-equilibrium phenomena in rarefied polyatomic gases: A high-order macroscopic model. *Phys. Fluids* **26** (5).

ROOHI, E., STEFANOV, S., SHOJA-SANI, A. & EJRAEI, H. 2018 A generalized form of the Bernoulli Trial collision scheme in DSMC: Derivation and evaluation. *J. Comput. Phys.* **354**, 476–492.

RYKOV, V. A. 1975 A model kinetic equation for a gas with rotational degrees of freedom. *Fluid Dyn.* **10** (6), 959–966.

SHARIPOV, F. 2006 Onsager-Casimir reciprocal relations based on the Boltzmann equation and gas-surface interaction: Single gas. *Phys. Rev. E* **73** (2), 026110.

24

721 SHARIPOV, F. & KALEMPA, D. 2008 Numerical modeling of the sound propagation through a rarefied gas
722   in a semi-infinite space on the basis of linearized kinetic equation. *J. Acoust. Soc. Am.* **124** (4),
723   1993–2001.
724 SHARIPOV, F., MARQUES JR, W. & KREMER, G. M. 2002 Free molecular sound propagation. *J. Acoust. Soc.*
725   *Am.* **112** (2), 395–401.
726 STRUCHTRUP, H. 2012 Resonance in rarefied gases. *Contin. Mech. Thermodyn.* **24**, 361–376.
727 SU, W., LI, Q., ZHANG, Y. & WU, L. 2022 Temperature jump and Knudsen layer in rarefied molecular gas.
728   *Phys. Fluids* **34** (3), 032010.
729 SU, W., WANG, P., ZHANG, Y. & WU, L. 2020 Implicit discontinuous Galerkin method for the Boltzmann
730   equation. *J. Sci. Comput.* **82**, 1–35.
731 SU, W., ZHANG, Y. & WU, L. 2021 Multiscale simulation of molecular gas flows by the general synthetic
732   iterative scheme. *Comput. Methods Appl. Mech. Eng.* **373**, 113548.
733 TANG, H., CHENG, P. & XU, K. 2001 Numerical simulations of resonant oscillations in a tube. *Numerical*
734   *Heat Transfer, Part A: Applications* **40** (1), 37–54.
735 TISZA, L. 1942 Supersonic absorption and Stokes' viscosity relation. *Phys. Rev.* **61** (7-8), 531.
736 WAGNER, W. 1992 A convergence proof for bird's direct simulation Monte Carlo method for the Boltzmann
737   equation. *J. Stat. Phys.* **66**, 1011–1044.
738 WANG, P., ZHU, L., SU, W., WU, L. & ZHANG, Y. 2018 Nonlinear oscillatory rarefied gas flow inside a
739   rectangular cavity. *Phys. Rev. E* **97** (4), 043103.
740 WANG, R. J. & XU, K. 2012 The study of sound wave propagation in rarefied gases using unified gas-kinetic
741   scheme. *Acta Mech. Sin.* **28** (4), 1022–1029.
742 WANG, Y., UBACHS, W. & VAN DE WATER, W. 2019 Bulk viscosity of CO2 from Rayleigh-Brillouin light
743   scattering spectroscopy at 532 nm. *J. Chem. Phys.* **150** (15).
744 WANG, Z., YAN, H., LI, Q. & XU, K. 2017 Unified gas-kinetic scheme for diatomic molecular flow with
745   translational, rotational, and vibrational modes. *J. Comput. Phys.* **350**, 237–259.
746 WANG-CHANG, C. S. & UHLENBECK, G. E. 1951 Transport phenomena in polyatomic gases. *Research Rep.*
747   *CM-681. University of Michigan Engineering* .
748 WU, L. 2016 Sound propagation through a rarefied gas in rectangular channels. *Phys. Rev. E* **94** (5), 053110.
749 WU, L., LI, Q., LIU, H. & UBACHS, W. 2020 Extraction of the translational Eucken factor from light scattering
750   by molecular gas. *J. Fluid Mech.* **901**, A23.
751 WU, L., REESE, J. M. & ZHANG, Y. 2014 Oscillatory rarefied gas flow inside rectangular cavities. *J. Fluid*
752   *Mech.* **748**, 350–367.
753 WU, L., WHITE, C., SCANLON, T. J., REESE, J. M. & ZHANG, Y. 2015 A kinetic model of the Boltzmann
754   equation for non-vibrating polyatomic gases. *J. Fluid Mech.* **763**, 24–50.
755 YANG, M. & SHENG, P. 2017 Sound absorption structures: From porous media to acoustic metamaterials.
756   *Annu. Rev. Mater. Res.* **47**, 83–114.